IJSRM
INTERNATIONAL JOURNAL OF SCIENCE AND RESEARCH METHODOLOGY
An Official Publication of Human Journals

Human Journals
Research Article
January 2018 Vol.:8, Issue:3

Exfoliated Graphite/Tungsten Trioxide Nanocomposite Electrode for the Photoelectrochemical Degradation of Eosin Yellow and Methylene Blue in Wastewater

IJSRM
INTERNATIONAL JOURNAL OF SCIENCE AND RESEARCH METHODOLOGY
An Official Publication of Human Journals

O. M Ama

Department of Applied Chemistry, University of Johannesburg, P.O. Box 17011, Doornfontein, 2028, South Africa.

Submission: 19 December 2017
Accepted: 29 December 2017
Published: 30 January 2018

Keywords: Exfoliated Graphite, WO_3 nanoparticle, Advance Oxidation Processes and Dyes

ABSTRACT

The exfoliated graphite /tungsten-trioxide (EG-WO_3) was prepared by incorporating WO_3 into EG by wet solution method. The materials were characterized using Scanning Electron Microscopy (SEM), Thermogravimetry, Differential Thermal Analysis (TGA), Brunauer-Emmett-Teller surface area analysis (BET), Infrared (IR) spectroscopy and X-ray Diffraction (XRD). These techniques confirmed the synthesis of EG-WO_3 nanocomposite. The EG-WO_3 was fabricated into a photoanode and applied to the photoelectrochemical degradation of eosin yellow dye as a model for organic pollutants in water at a current density of 7.2 mA cm^{-2} with Na_2SO_4 as supporting electrolyte. Was studied as a model material by photocatalytic and photoelectrochemical methods in order to evaluate the photoactivity of EG-WO_3 materials and the possibility of their applications in solar simulator photocatalysis. With the EG-WO_3 photoanode showed a significant decrease in the dye concentration (20 ppm). This shows that the WO_3 nanoparticle in the EG-WO_3 composite enhanced the degradation efficiency of the eosin yellow. Thus, the EG-WO_3 electrode is applicable for the photoelectrochemical oxidation of organic pollutants, specifically in synthetic dyes in water.

1. INTRODUCTION

Currently, there is increasing global demand for clean water and access to clean water is a major challenge in many countries due to population growth, drought and so on. Contamination of natural water as a result of industrial activities is a concern globally [1]. Many industries such as textile and printing are releasing large quantities of colored effluents containing unconsumed dyes, surfactants and sometimes traces of metals into water bodies [2, 3]. The disposal of these substances causes water pollution owing to their acute toxicity and thus their removal is of utmost importance. Dyes are highly visible material (even at low concentration), they possess high stability under sunlight and are resistant to microbial attack and temperature. Another challenging feature of most dyes is that they are not easily degradable or removed by conventional wastewater treatment plants [4]. Conventional water treatment techniques such as activated carbon adsorption, membranes filtration, ion exchange, coagulation/flocculation etc. can be expensive or involves the use of reagents or generate unwanted wastes that constitute additional burden to the environment. These shortcomings have led to the quest for alternative or complementary treatment techniques that are green, sustainable and cost effective in the removal of organic water pollutants. Advanced Oxidation Processes (AOPs) have gained much attention in this regard [5]. In recent years, photocatalysis and electrochemical oxidation techniques have gained wide popularity as alternatives for wastewater remediation [6]. Electrochemical oxidation is a clean, versatile and powerful tool for the destruction of organic compounds in water. But the generation of parasitic oxygen radical at certain potentials depletes the radicals needed for the destruction of organics and thus limits the efficiency of the method.

In photocatalysis, hydroxyl radicals are generated when light of certain wavelength is incident on the photocatalytic materials. These radicals react with the target pollutant and cause its degradation/mineralization. However, wideband gaps of many photoactive semiconducting metal oxides make them operate effectively in the UV region only. Consequently, efforts to harness the potential of the sun in water remediation *via* photocatalysis suffers a setback. Furthermore, these photocatalysts are also known to be affected by electron-hole recombination, which impacts negatively on their photocatalytic performance. Combination of electrochemical oxidation and photocatalytic process not only maximizes production of the needed oxidant but also ameliorates the challenge of electro-hole recombination as the excited electron is channeled away via the cathode. In addition, the

photogenerated electrons can reduce the undesirable oxygen molecule evolved in an electrochemical process to superoxide.

A typical combination of heterogeneous photocatalysis and electrochemical oxidation involves the immobilization of a photoactive material such as WO_3 powder on a conducting material such as exfoliated graphite [7].

It should be noted that graphite is naturally abundant, cheap, stable and environmental friendly [8]. The immobilization of the catalyst has several advantages, such as an enhanced photocatalytic efficiency and the avoidance of losses in the recovery process through the use of an external electric field. Due to the fact that both the photoactive material (photocatalyst) and the conducting material (electrode) can simultaneously generate hydroxyl (OH^-) radicals, the combination of electrochemical and photocatalytic oxidation techniques guarantees an increased removal capacity. The generated OH^-radicals are among the active species for the decomposition of organic dyes in wastewater [9]. To prevent the photocatalyst from falling off and thus prolong the lifetime of photoelectrode in the photoelectrochemical system, the applied potential at the anode should be kept low. However, the use of very low anodic potentials can significantly decrease the effectiveness of the electrochemical oxidation process. Hence, photoelectrochemical oxidation methods for the mineralization and degradation of organic pollutants should be optimized to improve the stability and photoefficiency of the method [10].

2. MATERIALS AND METHODS

2.1 Materials / Apparatus

Exfoliated graphite (EG), eosin yellowish dye, ethylene glycol, nitric acid, Ammonium Metatungstate (AMT), and sulfuric acid were purchased from Sigma-Aldrich while WO_3 was synthesized. The characterization of EG and the composite were carried out using Scanning Electron Microscopy (SEM) with energy-dispersive X-ray spectroscopy microanalysis (VGA3 TESCAN), Brunauer–Emmett–Teller (BET) nitrogen adsorption–desorption (Shimadzu, Micromeritics ASAP 2010 Instrument), UV–Vis diffuse reflectance spectroscopy (Shimadzu 2450) of dry powders using $BaSO_4$ was used as a reflectance standard, X-ray diffractometer (Bruker D8 with Cu-Kα), and Raman spectroscopy (Lab RAM HIR, HoridaJobinXvon, France using 514.5 nm air cooled with Ar+Laser) with ×50 objective and laser intensity of 1.3 mW.

The photocatalytic experiment was performed using New Port 9600 Full Spectrum Solar Simulator equipped with a 400-W ozone-free xenon lamp which produces a collimated beam of 33-mm diameter. The distance between the simulator and the reaction vessel was set at a distance of 10 cm to produce a beam power equivalent to 1 sun. The experiments were carried out in a photoreactor with an approximate volume of 100 mL of the dye solution. The working electrodes EG and EG-WO_3 with 1 cm^2 areas were used, as well as Ag/AgCl (3.0 M KCl) and platinum foil as a reference and counter electrode respectively. A computer-controlled potentiostat was employed as the power source for the electrochemical degradation of Eosin Yellowish dye (60 mL) prepared in a 0.1 M sodium sulfate-supporting electrolyte. Aliquots were taken at 30 min intervals from the electrochemical/photoelectrochemical cell. Decrease in the concentration of the dye was followed on UV-Vis (PerkinElmer model Lambda 35) at the wavelength of maximum absorbance of the dye (516 nm) Parameters, including the effect of the WO_3 loading, the pH value of the solution, the current density (7.5–15 mA), initial concentration (0–0.8 mM), and applied potential on the degradation efficiency of WO_3 were investigated.

2.2 Synthesis of tungsten trioxide

1 g of AMT was added to 60 ml of deionized water in a beaker. The mixture was stirred for few minutes and left to dissolve, polyethylene glycol (0.5 mL) was added dropwise and stirred for 30 min. The pH of the mixture neutral. The mixture was centrifuged and the obtained solid was dried in an oven at 100ºC overnight. The dried powder was calcined at 500°C for 3 h.

2.3 Preparation of Composite Material

Exfoliated graphite (10 g) was added to 1g of WO_3 nanoparticles in deionized water and the mixture was stirred for 12h and sonicated for 3h. The resultant mixture was then dried overnight in an oven at 50°C to obtain the EG–WO_3 nanocomposite. The composite was finally compressed into a pellet and fabricated into an electrode.

2.4 Fabrication of the Electrode

To fabricate an electrode, 150 mg of exfoliated graphite was compressed at high pressure to form a pellet of 1cm diameter. Using a glass tube with conduction silver paint, a copper wire was then coiled on one end to form a flat surface. Therefore, the as-prepared EG pellet was

cut into a smaller size and then place on the surface of the coiled copper wire using epoxy resin. Therefore, the contribution of current is only from the basal plane for transmission of electrons to the external circuit.

2.5 Degradation Experiments

The degradation method involves the degradation study and kinetics of the dye. The distance between the experimental setup and the simulator was set at a distance of 10 cm to produce a beam power equivalent to 1 sun. Furthermore, a galvanostatic/ potentiostat with a current density (7.2–15 mA), initial concentration (0-0.8mM) the power supply is employed for the electrochemical degradation of the dye in 0.1 M sodium sulfate supporting EG and EG – WO_3 with 1 cm^2 areas were used as working electrodes, Ag/AgCl (3.0M KCl) and platinum foil as a reference. The working electrode surface was then aligned to receive the beam of light coming from the solar simulator. In addition, all degradation experiments were performed in a cell containing the eosin yellowish solution and the photoanode. To investigate the degradation of the dye, photoelectrochemistry, photolysis and electrochemistry processes were carried out. In these processes, both potential and light were used in the cell, only light was employed for photolysis, and only potential without solar simulation was used for electrochemical oxidation. To monitor the extent of degradation, the aliquots of the suspended samples (5 ml) were taken at 30-min intervals for about 180 h 20, using syringe and filtered through a 0.4-μm polyvinylidene fluoride (PVDF) membrane filter.

3. RESULTS AND DISCUSSION

Characterization of exfoliated graphite and WO_3 composite material

3.1 Scanning electron microscopy (SEM)

Fig. 1(a) and 1(b) show SEM images of the as-prepared WO_3 and EG-WO_3 nanocomposite respectively. The presence of WO_3 particle where seen as white particles spread uniformly throughout, (Fig.1c). Throughout EDX also indicate the presence of WO_3.

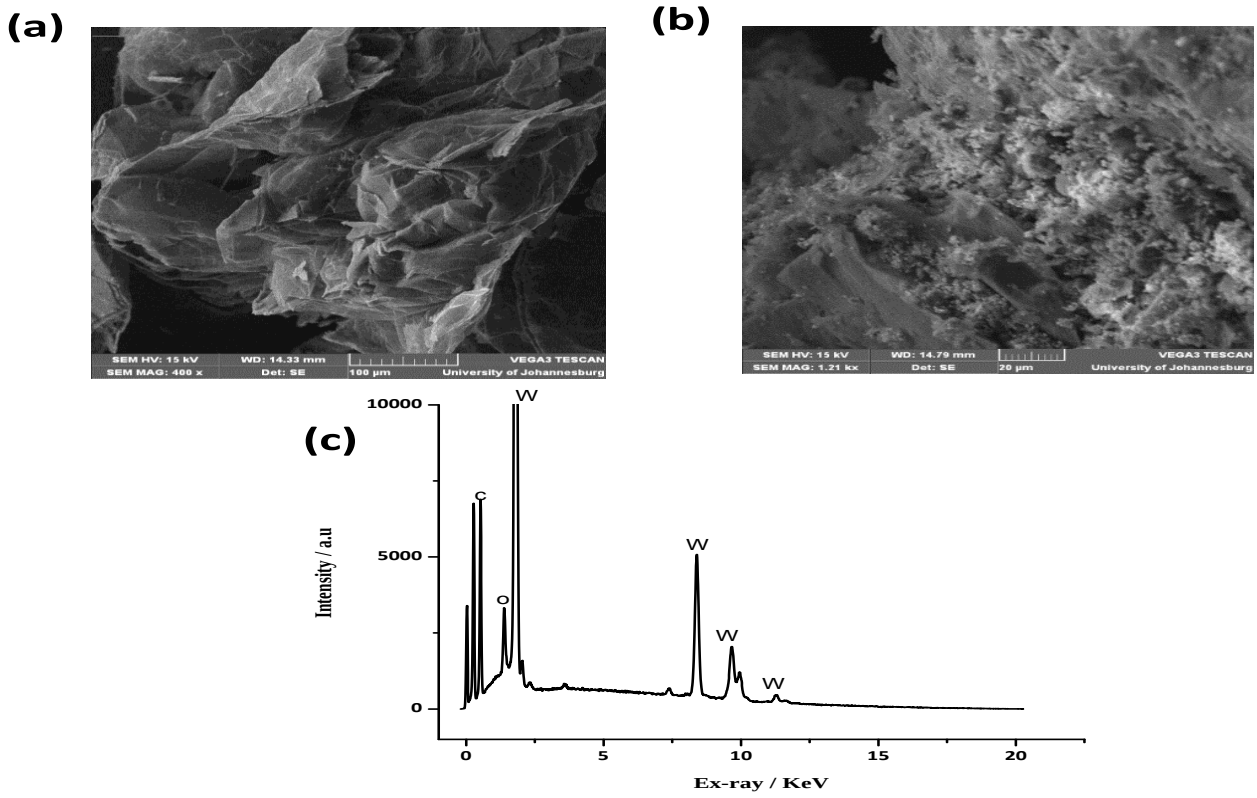

Fig. 1: SEM images of: (a) EG, (b) EG-WO_3. (C) EDX spectrum of EG-WO_3.

3.2 Raman Spectroscopy

Fig. 2a shows the Raman spectrum of WO_3. The Raman peaks appearing at 713 and 803 cm^{-1}represent the anatase phase of WO_3. The spectrum of the EG–WO_3 is shown in Fig. 2b. The peak at 1045 cm^{-1} corresponds to D band which relates to E_{2g} photon vibration of SP^2 carbon, while the peak at 1065 cm^{-1} agrees with the G band of the EG. The peaks located at 711, 753, 800, 807 and 930 cm^{-1} are attributed to the Raman vibrational modes of WO_3. The appearance of the WO_3 vibrational modes is an indication of the successful fabrication of the EG-WO_3 nanocomposite [11].

Fig. 2c reveals the XRD pattern of nanocrystalline WO_3 annealed at 500 °C. The XRD pattern shows that the WO_3 powder contains both monoclinic and tetragonal phases, corresponding to JCPDS 32-1154 [12]. The thermoclinic face is the major face. In addition, the sizes of the materials were then obtained using the Debye-Scherrer equation The sizes of the materials were then obtained using the Debye-Scherrer equation $D = \frac{K\lambda}{\beta\cos\theta}$ where D is the crystalline size, K is a constant 0.9, λ is the wavelength of the x-rays, and β is the full width of half maximum of the diffraction peak in unit of radian and θ is the Bragg angle. The calculated

crystalline sizes of the WO_3 were 20 nm. The XRD pattern of the EG consists of characteristic peak of EG occurring at 2θ = 24.61.The characteristic peaks of EG and WO_3 in the XRD patterns indicate the formation of EG-WO_3composite. The dilution caused by the presence of EG reduce intensity of WO_3 as shown in fig. 2c.

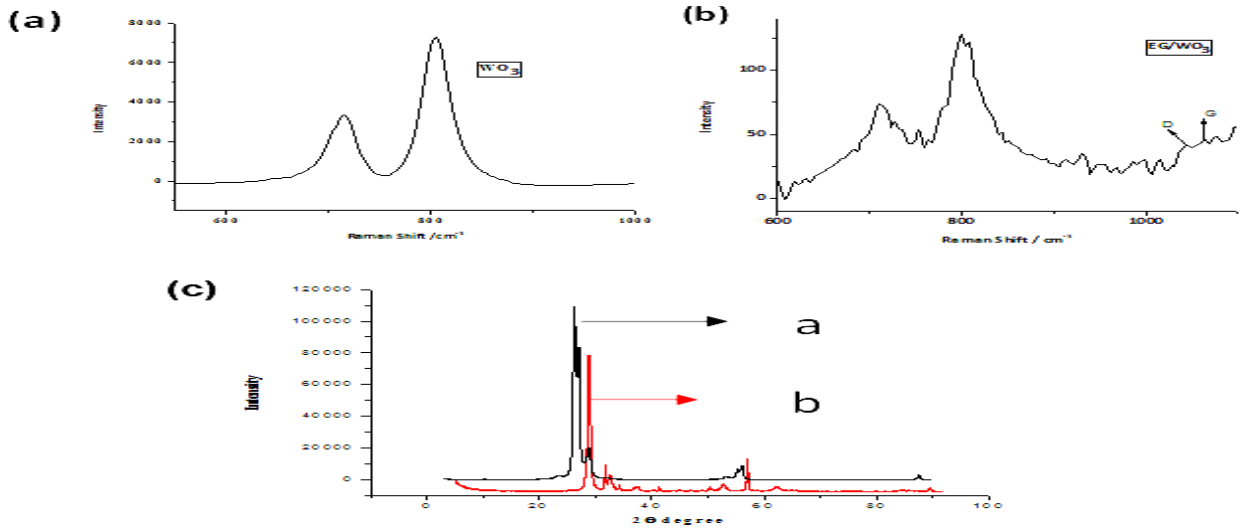

Fig. 2: Raman spectra of (2a) WO_3 and (2b) exfoliated graphite- WO_3 materials (2c) XRD pattern of (a) WO_3 and (b) EG-WO_3 materials

3.3 Infrared (IR) spectroscopy

FT-IR spectra of exfoliated graphite EG, EG-WO_3 nanocomposite are shown in Fig. 3a. The EG shows OH broad peak at 3426 cm^{-1} which are as a result of adsorbed water molecules; C=C peak at 1643 cm^{-1} which is assigned to the skeletal vibration of EG. EG-WO_3 showed numerous characteristic peaks of O-H-O out of plane wagging at 829 cm^{-1}, OH vibration at 3406 cm^{-1}; C-O stretching mixed with C-OH bending at 1067 cm^{-1}, C=O stretching at 1384 cm^{-1}; epoxy symmetrical ring deformation at 1192 cm^{-1}, OH deformation at 1125 cm^{-1} and C=C skeletal vibration from unoxidized graphitic domain at 1627 cm^{-1} [13]. Fig.(3b) show the UV result, which highlights the photocatalytic property from Uv-diffusion reflectance of WO_3 and the characteristic band of WO_3 which is below 310 nm (Fig 3b). This shows a comparison of the optical absorption edge of the EG-WO_3 nanocomposite. For the EG-WO_3 composite, the spectra display an enhanced absorption in the visible region (λ>420 nm). Hence, EG presence in the composite resulted in redshift of the absorption edge due to photosensitizer role play by EG. Therefore, the immobilization of EG improves visible light

absorbance, which emphasizes the synergistic effect of EG. Hence, the EG-WO_3 electrode was an ideal composite for the degradation experiment.

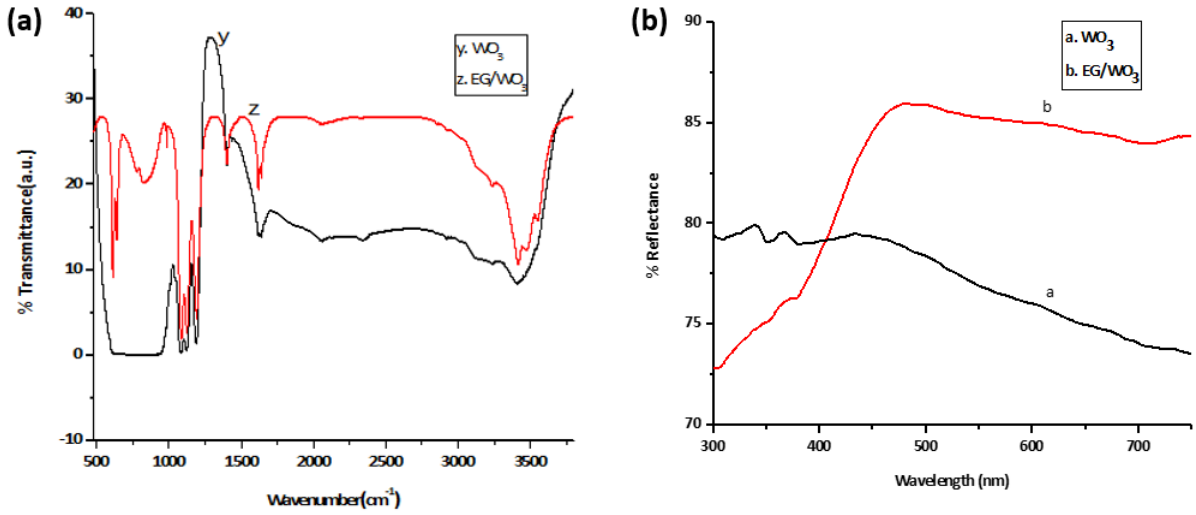

Fig. 3: (a) FT-IR spectra of WO_3 (y) and exfoliated graphite-WO_3, (z) materials. (b) The UV-Vis diffuse reflectance spectra of EG, and (c) EG-WO_3

3.4 BET

Table 1 shows the BET surface area of EG and EG-WO_3 nanocomposites. The WO_3 was doped with EG. Therefore, the EG-WO_3 sample shows an increase in the BET the pore volume and surface area than those of the EG. The increase in the surface area of the nanocomposites could be useful in the photocatalytic process, which might efficiently transport the pollutant in the solution to the catalyst surface to improved photoelectrochemical oxidation activity.

Table 1 BET data of EG, WO_3 and EG-WO_3

Sample	BET Surface Area/M^2g^{-1}	Pore Volume/CM^3g^{-1}
EG	13.96	0.026
WO_3	27.30	0.056
EG-WO_3	15.95	0.015

3.5 Electrochemical Characterization of the EG and EG-WO_3

The electrochemical properties of EG and EG-WO_3 electrodes were examined by carrying out cyclic voltammetry using potassium ferricyanide as a redox probe. Fig. 4 shows the cyclic

voltammogram obtained for 5 mM $[Fe(CN)_6]^{-3/-4}$ in 0.1 M KNO_3 at (a) EG and (b) EG-WO_3 electrodes. The EG electrode displays the characteristic voltammetric response for $[Fe(CN)_6]^{-3/-4}$ with a peak-to-peak separation of 135 mV (Fig 4a) whereas the EG-WO_3 electrode produces a voltammetric response for $[Fe(CN)_6]^{-3/-4}$ with a peak-to-peak separation of 205 mV. Hence EG electrode exhibits lower electron transfer kinetics than EG-WO_3 electrode. The higher electron transfer kinetics of EG-WO_3 can be attributed to the synergic effects of EG, $[Fe(CN)_6]^{-3/-4}$ and WO_3 since these materials are known to exhibit photoelectrochemical properties.

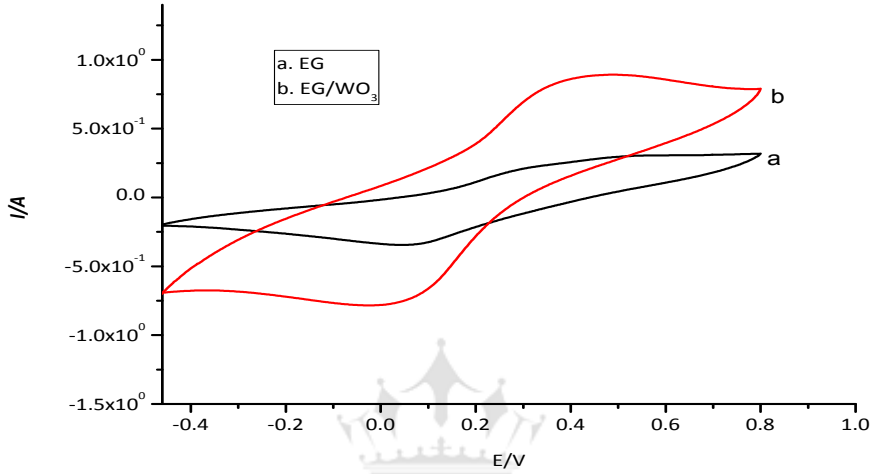

Fig. 4: Cyclic voltammograms of (a) EG and (b) EG-WO_3 electrodes in 5 mM $[Fe(CN)_6]^{-4}$ at 20 mV s^{-1}.

4. Photoelectrochemical Procedure

The EG-WO_3 was used as electrode for the photoelectrochemical degradation of eosin yellow dye and a removal efficiency of 88.33 % was obtained after 180 min electrolysis time, at the optimum conditions of pH 7, a relatively mild 2.5 V potential and low current density, which suggest the suitability of the prepared EG-WO_3 as a photoanode in the photoelectrochemical degradation of Eosin yellow dye [14].

Further results were obtained by using the Langmuir-Hinshelwood model to determine the photoelectrochemical performance of the composite wherein the following equation was applied:

$$\ln C_o/C_t = kt \qquad (1)$$

Where C_o/C_t is the normalized concentration, t is the reaction time, and k is the apparent reaction rate constant. The k value for the photoelectrochemical method was $4.23\times10^{-1}min^{-1}$ and $5.75\times10^{-3}min^{-1}$ for the EG-WO_3 and bare WO_3 respectively.

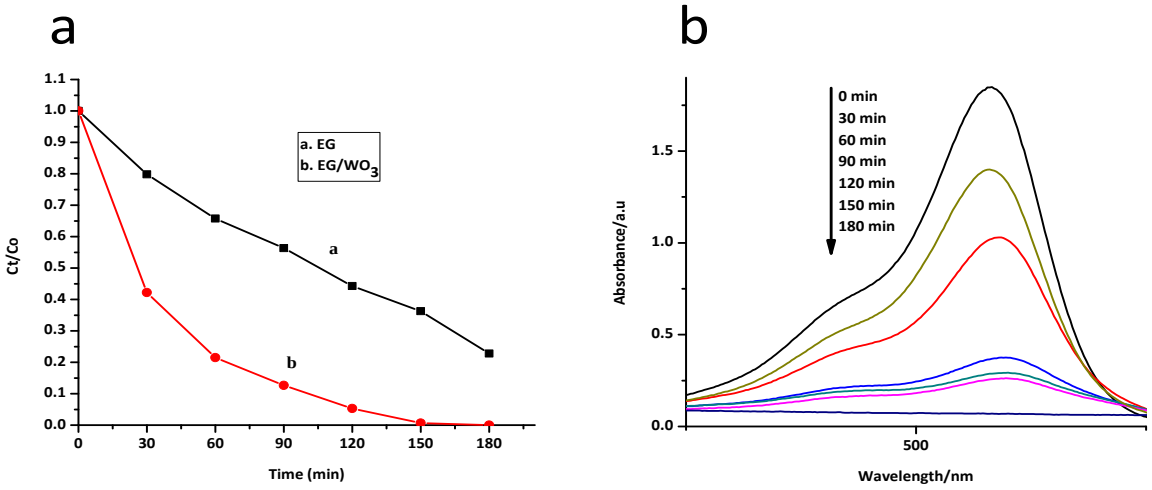

Fig. 5: (a) Degradation of Eosin Yellow in the first 180 m in (b) Uv-Vis spectra showing the Degradation Profile of Eosin Yellowish.

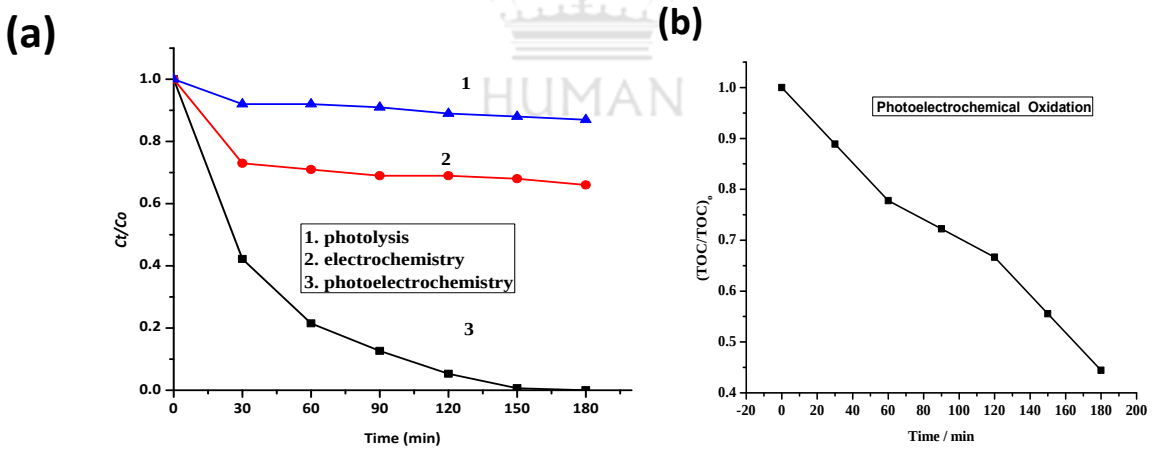

Fig. 6: Normalized concentration decay Curve of 0.1 × 10−4 M Eosin Y during (a1) Photolysis, (a2) electrochemical oxidation and (a3) photoelectrochemical oxidation and (6b) TOC showing the (Photoelectrochemical Degradation).

This indicates bare EG-WO_3 can degrade the dye faster than the EG pristine. Like the EG-ZrO2, the EG-WO3 photoelectrochemical degradation of eosin yellowish dye followed a pseudo first order kinetics. The photoelectrochemical method (Fig 6a3) was compared to both photocatalysis, EG-WO_3 in the absence of potential and electrochemical oxidation, the EG-

WO_3 in the absence of light shown in (Fig 6a2), both photolysis and electrochemical oxidation showed low removal of the dye in comparison to the photoelectrochemical oxidation. The photoelectrochemical oxidation reaction is normally initiated after hydroxyl groups have been adsorbed onto the electrode's surface. The interaction between the hydroxyl groups and the electrode results in the formation of hydroxyl radical. Once generated, the hydroxyl radicals attack and oxidize the pollutant resulting in the degradation of the pollutant. However, there is a high propensity for the generated hydroxyl radicals to react with each other and produce oxygen molecules. This side reaction (oxygen molecule generation) reduces the number of hydroxyl radicals available for effective degradation of the pollutant. In addition, the generated oxygen molecules have the tendency to form a barrier between the hydroxyl radicals and the pollutant and interfere with the degradation process. The poor degradation efficiency of the photolysis process is attributed to High charge carrier recombination rate. Photoelectrochemical oxidation showed a synergic improvement over the other two methods with a removal efficiency of about 88.33%. The high photoelectrochemical oxidation performance of the EG-WO_3 could be as a result of the delayed electron–hole recombination due to trapping of electrons in the conduction band by EG orbital and efficient transfer of the charge carriers. The oxygen molecules released during electrochemical process is known to act as an electron acceptor for oxidation during photolysis, thereby promoting the rate of degradation through indirect oxidation [15]. Again, the photo-catalyst used in this composite WO_3 has the potential to produce hydroxyl radicals when irradiated with light of the appropriate energy and hence improving the overall efficiency of the composite [12]. Combination of the electrochemical oxidation method with photolysis is therefore regarded as an effective technique since the oxygen molecules produced as by-products during electrolysis is employed to augment the efficiency of the photolysis process. This accounted for the improved degradation efficiency of the dye by the EG-WO_3 composite[10]. Fig. (6b) shows the Total Organic Compound (TOC) measurement of the degradation achieved by oxidizing the degradation sample using different time intervals. TOC analysis measures the degree of carbon mineralization during degradation technique of the organic dye in water [15]. Therefore, the extent of mineralization was highest in the photoelectrochemical procedure with a value of Ca 70%. [16].

4.1 Photoelectrochemical Degradation of Methylene Blue

Methylene blue dye was used to determine the photoelectrochemical degradation ability of the EG-WO_3 electrode. UV-Vis spectrophotometer was used to monitor the dye removal efficiency. Fig. 7 (a & b) represent the extent of dye degradation by using EG, and EG-WO_3 respectively. Fig. 7b specifies a major dye degradation efficiency in relation to the pure EG Fig. 7a indicating the significant effect of the WO_3 in the nanocomposite. With dye degradation efficiency of 79.11 % in just 180 minutes at conditions of neutral pH and the prepared EG-WO_3 photoanode is considered to be suitable for the photoelectrochemical degradation of methylene blue dye. Langmuir-Hinshelwood's model: $\ln C_0 / C_t = kt$ Was used to interrogate the dye degradation kinetics. Where C_o/Ct is the normalized concentration, t is there action time, and k is the apparent reaction rate constant. The result of this analysis is presented in Fig. 7c. The degradation process occurred according to pseudo first order kinetics.

The dye degradation was also performed through photocatalysis, and electrochemical oxidation methods and the results compared to that of photoelectrochemical method. The photocatalytic degradation involved the use of EG-WO_3 without the application of potential. On the other hand, the electrochemical oxidation method employed EG-WO_3 without light. Fig. 8 (a, b & c) represents the UV-Vis spectra of methylene blue dye degradation by photoelectrochemical, photocatalysis, and electrochemical oxidation methods respectively. The normalized concentration decay curve of the dye using photoelectrochemical, photocatalysis, and photo oxidation methods are also depicted in Fig. 8d (a, b, c) respectively. Compared to the photoelectrochemical oxidation, photolysis and electrochemical oxidation showed minimal dye removal efficiency.

Delete down in electrochemical oxidation process, hydroxyl radical formation occurs as a result of adsorption of OH molecules on electrode's surface. The OH groups, after adsorption, tends to react among themselves and produce oxygen molecules. Deactivation of hydroxyl radical can result in poor degradation efficiency since it is these radicals that cause the oxidation of the organic pollutants. Again, the oxygen molecules can also interfere with the reaction between pollutant and the hydroxyl radical and hamper the degradation process. Charge carrier recombination is believed to be the cause for the poor performance of the photolysis process. Photoelectrochemical oxidation showed improved performance and

displayed 79.11% efficiency. This high efficiency displayed by the EG-WO_3 is the outcome of delayed electron-hole recombination due to the trapping of electrons in the conduction band by EG orbital. The tendency of the oxygen molecules released by the electrochemical technique to act as electron acceptors for oxidation in the photolysis process has been reported to promote the degradation rate by indirect oxidation [12]. The WO_3 used in our composite, further to this possibility, has the tendency to produce hydroxyl radicals when illuminated with light of appropriate energy, hence the resultant high degradation efficiency [15]. Combination of photolysis and electrochemical oxidation system has the advantage of utilizing the oxygen molecules produced during electrolysis to improve the efficiency of photolysis process. This occurrence enhances the degradation efficiency of EG-WO_3. Replace with the mechanism of photoelectrochemical degradation, in this case, is similar to that discussed earlier for the EG-WO_3 Eosin yellowish.

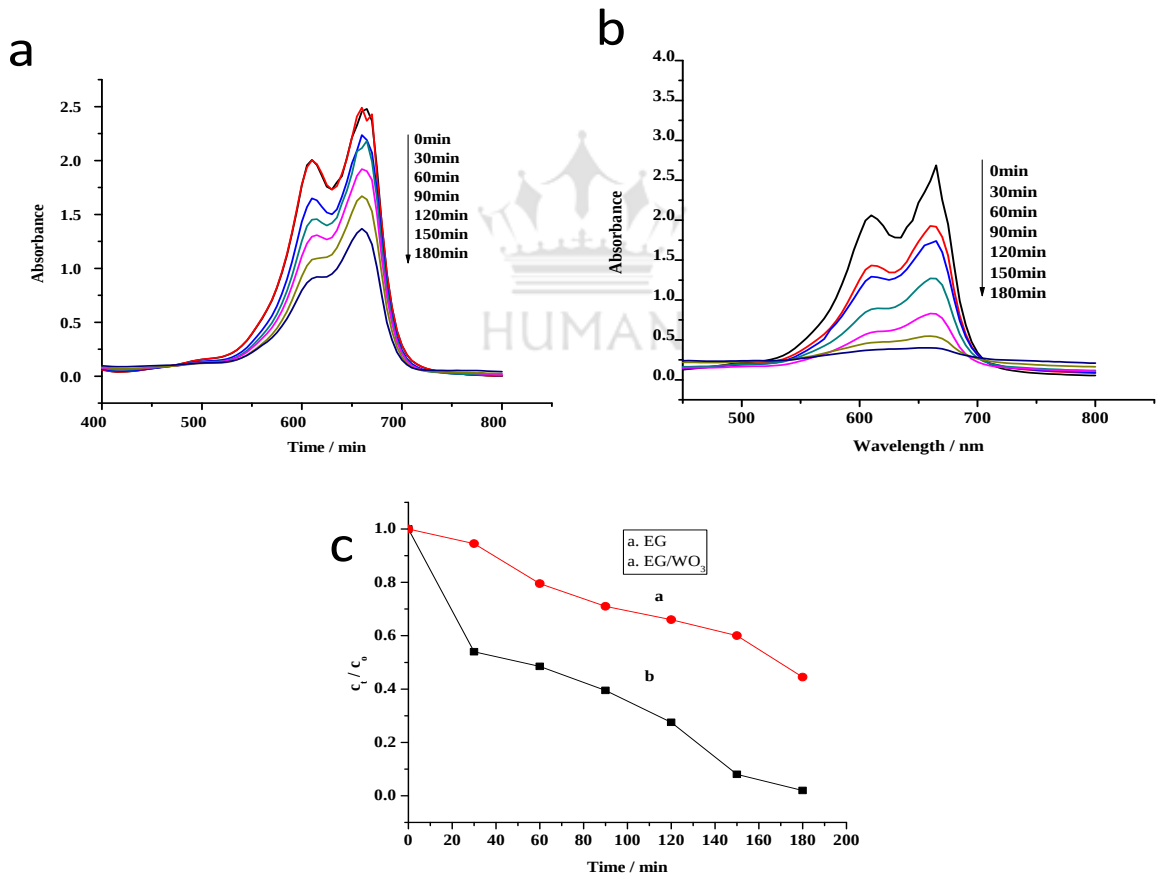

Fig. 7: UV-Vis spectra during degradation of 0.3 x 10^{-4} M Methylene blue at (a) EG photoelectrochemical (b) EG-WO_3 photoelectrochemical oxidation and (c) Normalized concentration decay curve for the photoelectrochemical degradation.

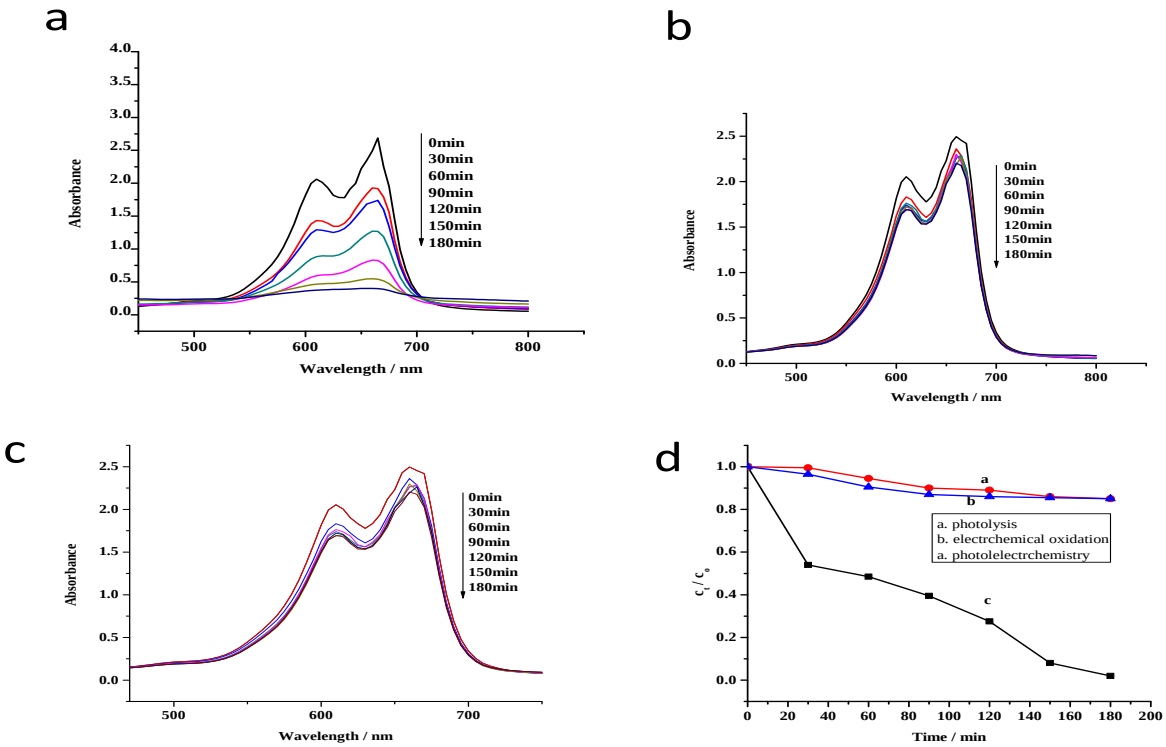

Fig. 8: UV-Vis spectra profile during (a) photolysis (b) electrochemical (c) photoelectrochemical degradation of 0.3 x 10^{-4} M Methylene blue Dye. (d) Normalized concentration decay curve of 20 ppm methylene blue dye in 0.1 M Na_2SO_4 solution under (i) photolysis (ii) electrochemical oxidation (iii) photoelectrochemical oxidation

5 Total Organic Carbon (TOC) Measurement

Fig. 9 shows, at different time intervals, the TOC analysis of the degraded dye. The TOC result shows the extent of the mineralization of carbon during the oxidation/degradation of the organic dye in water [16]. High degree of mineralization of the dye was observed with a value of Ca 65%. The high TOC value obtained in this analysis indicates the effectiveness of the composite incomplete mineralization of the dye.

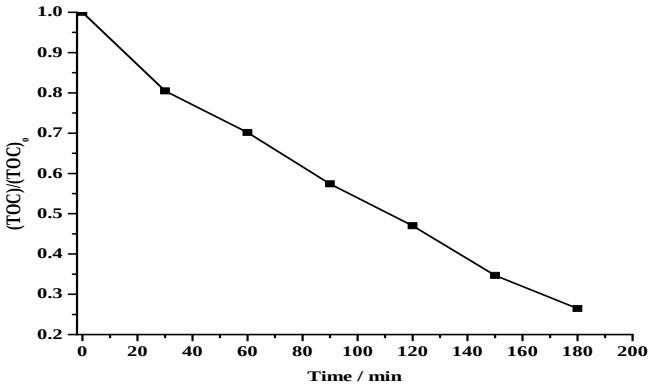

Figure 9 TOC measurements during photoelectrochemistry

6 CONCLUSION

EG-WO_3 has been successfully synthesized and applied in the photoelectrochemical degradation of Eosin yellowish and methylene blue dyes in water using simulated sunlight. The low cost of natural graphite and ease of preparation of the EG-WO_3 electrode possibly could lead to large-scale applications. The removal efficiency of 88.33 % of Eosin yellow and 79.11 % of methylene blue after just 180 minutes at the optimum conditions of neutral pH, showed the suitability of the prepared EG-WO_3 as a photoanode in the photoelectrochemical degradation of Eosin yellow and methylene dyes.

7 REFERENCES

[1] P.H. Gleick, N. Ajami, J. Christian-Smith, H. Cooley, K. Donnelly, J. Fulton, M.-L. Ha, M. Heberger, E. Moore, J. Morrison, S. Orr, P. Schulte, V. Srinivasan, The World's Water Volume 8: The Biennial Report on Freshwater Resources, Island Press 2014.

[2] A. Sarkar, Global Climate Change, Emissions Trading and Sustainable Energy Development, Asia Pacific Business Review, 6 (2010) 42-66.

[3] Z. Carmen, S. Daniela, Textile organic dyes-characteristics, pollution effects and separation/elimination procedures from industrial effluents- a critical overview, Intech Open Science, 2012.

[4] H. Abdullah, D.-H. Kuo, Y.-R. Kuo, F.-A. Yu, K.-B. Cheng, Facile synthesis and recyclability of thin nylon film-supported n-type ZnO/p-Type Ag_2O nano composite for visible light photocatalytic degradation of organic dye, The Journal of Physical Chemistry, DOI (2016).

[5] S.H.S. Chan, T. Yeong Wu, J.C. Juan, C.Y. Teh, Recent developments of metal oxide semiconductors as photocatalysts in advanced oxidation processes (AOPs) for treatment of dye waste-water, Journal of Chemical Technology and Biotechnology, 86 (2011) 1130-1158.

[6] E. Aazam, Photocatalytic oxidation of methylene blue dye under visible light by Ni doped Ag_2S nanoparticles, Journal of Industrial and Engineering Chemistry, 20 (2014) 4033-4038.

[7] K. Kalantar-Zadeh, A. Vijayaraghavan, M.-H. Ham, H. Zheng, M. Breedon, M.S. Strano, Synthesis of atomically thin WO_3 sheets from hydrated tungsten trioxide, Chemistry of Materials, 22 (2010) 5660-5666.

[8 G.C. Pradhan, S.] K. Swain, Graphite-reinforced oxygen barrier conducting starch bionanocomposites, Polymer Composites, 37 (2016) 2083–2091.

[9] Y. Cui, Z. Ding, P. Liu, M. Antonietti, X. Fu, X. Wang, Metal-free activation of H_2O_2 by g-C_3N_4 under visible light irradiation for the degradation of organic pollutants, Physical Chemistry Chemical Physics, 14 (2012) 1455-1462.
[10] O. Ama, N. Mabuba, O. Arotiba, Synthesis, Characterization, and Application of Exfoliated Graphite/Zirconium Nanocomposite Electrode for the Photoelectrochemical Degradation of Organic Dye in Water, Electrocatalysis, 6 (2015) 390-397.
[11] Y. Gui, J. Zhao, W. Wang, J. Tian, M. Zhao, Synthesis of hemispherical WO_3/graphene nanocomposite by a microwave-assisted hydrothermal method and the gas-sensing properties to triethylamine, Materials Letters, 155 (2015) 4-7.
[12] T. An, W. Zhang, X. Xiao, G. Sheng, J. Fu, X. Zhu, Photoelectrocatalytic degradation of quinoline with a novel three-dimensional electrode-packed bed photocatalytic reactor, Journal of Photochemistry and Photobiology A: Chemistry, 161 (2004) 233-242.
[13] B. Ntsendwana, B. Mamba, S. Sampath, O. Arotiba, Electrochemical detection of bisphenol A using graphene-modified glassy carbon electrode, Int J Electrochemical Science, 7 (2012) 3501-3512.
[14] S. Park, S. Lee, D. Kim, C.W. Lee, I.-S. Cho, K.S. Hong, Fabrication of TiO_2/tin-doped indium oxide-based photoelectrode coated with overlayer materials and its photoelectrochemical behavior, Journal of nanoscience and nanotechnology, 12 (2012) 1390-1394.
[15] T. An, Y. Xiong, G. Li, C. Zha, X. Zhu, Synergetic effect in degradation of formic acid using a new photoelectrochemical reactor, Journal of Photochemistry and Photobiology A: Chemistry, 152 (2002) 155-165.
[16] E. Brillas, C.A. Martínez-Huitle, Decontamination of wastewaters containing synthetic organic dyes by electrochemical methods. An updated review, Applied Catalysis B: Environmental, 166 (2015) 603-643.